Electronic Supplementary Information

Highly efficient bimetal synergetic catalysis of multi-wall carbon nanotubes supported palladium and nickel on hydrogen storage of magnesium hydride

Jianguang Yuan, Yunfeng Zhu and Liquan Li**

College of Materials Science and Engineering, Nanjing Tech University, 5 Xinmofan Road, Nanjing, 210009, P.R. China. E-mail: yfzhu@njtech.edu.cn; lilq@njtech.edu.cn; Tel: +86-25-83587255

Experimental

Original powders of Mg (99.72 wt.% in purity and <100 μm in size), $PdCl_2$ (AR, 99 wt.% in purity), $Ni(NO_3)_2 \cdot 6H_2O$ (AR, 99 wt.% in purity), ethylene glycol (CP, 98 wt.% in purity) and multi-walled carbon nanotubes (>97 wt.% in purity and 40-60 nm in external diameter) were commercially gotten.

MWCNTs treatment

The surface of MWCNTs was treated to ensure functionalization. MWCNTs were added to 50 ml concentrated nitric acid under stirring in an oil bath, with an increase in the temperature to 413 K. It was further refluxed and stirred for 6 h to remove impurities, and washed with distilled water till the PH value of the rinsed solution reached around 7, and finally dried under vacuum.

Preparation of Ni/MWCNTs catalyst

Ni/MWCNTs (mass ratio = 3:4) was synthesized by a chemical reduction method of an annealing process. MWCNTs and $NiNO_3 \cdot 6H_2O$ were dispersed into ethyl alcohol by ultrasonic vibration for 1h, followed by drying in blowing dry oven

at 358 K for 8h. Finally, the mixture was heat-treated at 673 K and held for 4 h in a tube furnace under Ar atmosphere. It was then heated up to 723 K and held for 4 h under H_2 atmosphere to ensure complete reduction of Ni. The sample was labeled as Ni_3/MWCNTs$_4$.

Preparation of PdNi/MWCNTs catalyst

PdNi/MWCNTs was synthesized by a solution chemical reduction method. The as-synthesized Ni_3/MWCNTs$_4$ was dispersed into ethylene glycol by ultrasonic vibration for 1h. Further, the required proper amount of aqueous solution of $PdCl_2$ was added to the solution under the condition of magnetic stirring for 4h. The PH of the entire solution was adjusted to more than 10 by adding NaOH (2.5 M), and the solution was refluxed and magnetic stirred in an oil bath at 383 K for 6 h to ensure complete reduction of Pd. In this reaction as the formula (1), ethylene glycol acted as a reducing, stabilizing, and dispersing agent. Finally, the suspension was filtered and the solid was washed with distilled water repeatedly until neutral and dried in blowing dry oven at 358 K. The sample was labeled as Pd_3Ni_3/MWCNTs$_4$.

$$x\mathrm{Pd}^{2+} + x\mathrm{H_2(HO)CC(OH)H_2} \xrightarrow{\mathrm{NaOH}/\triangle} \mathrm{Pd}_X - \mathrm{colloids} + x\mathrm{(HO)CC(OH)H_2} + 2x\mathrm{H}^+ \quad (1)$$

Preparation of Mg- PdNi/MWCNTs composite

The as-synthesized Pd_3Ni_3/MWCNTs$_4$ and Mg mixed in a certain molar ratio (5:95) were homogenized by ultrasonic vibration in acetone for 30 min. After being completely dried in air, the powders were directly used for HCS. During the HCS process, the samples were first heated up to 853 K at a heating rate of 10 K/min under

2 MPa hydrogen atmosphere and kept at that temperature for 1 h. It was then cooled down to 613 K and held for 4 h. Finally, the sample was cooled down to room temperature. Afterward, the HCS product was mechanically milled for 10 h in a stainless steel vial with stainless steel balls under Ar atmosphere with the ball to powder ratio of 30:1. MM was conducted with a 400 r/min milling rate by a planetary milling apparatus. The as-prepared HCS products were denoted as Mg_{95}-$(Pd_3Ni_3/MWCNTs_4)_5$. To verify the bimetal synergetic catalysis in this study, three samples of Mg_{95}-$(Pd_6/MWCNTs_4)_5$, Mg_{95}-$(Ni_6/MWCNTs_4)_5$ and Mg were prepared by the above- mentioned method.

Sample characterization

The microstructures of the catalysts, HCS and HCS + MM products were examined by means of X-ray diffraction (XRD) with Cu-K_α radiation (40 kV and 35 mA), scanning electron microscopy (SEM, JEOL JSM-6360LV) and high-resolution transmission electron microscope (HRTEM, JEM-2010 UHR). X-ray photoelectron spectroscopy (XPS) was carried out in a Perkin Elmer PHI 550 multi-technique spectrometer with the electron gun Perkin Elmer PHI 25-270AR precision electron analyzer. Data acquisition took place in the constant energy analyzer mode with a pass energy of $\triangle E = 50$ eV and Al Kα radiation from a monochromatic aluminum X-ray source. The sample was mixed with silicon dioxide and tableted before testing. The binding energy calibration was performed on the silicon Si 2p peak with the energy of 103.4 eV. The software Rietica was used for the quantitative phase analysis of the HCS product based on the Rietveld method. The average grain sizes of the

main phase MgH_2 in the composites were estimated from the XRD patterns according to scherrer's equation:

$$D\,\beta\,\cos\theta\;=\;0.9\,\lambda \qquad (2)$$

where D is the grain size, λ is the X-ray wavelength of 0.154 nm, β is the full width at half maximum of the diffraction peak and θ is the Bragg angle. Samples of TEM characterization were prepared by ultrasonic shaking of the powder in ethanol and drying it on a copper grid with a holey carbon foil.

The hydrogen storage properties of the HCS + MM products were measured by a Sieverts type apparatus (GRC, Advanced Materials Co.). About 0.5 g of the powders was loaded into a stainless steel sample chamber in the glove box filled with argon. Since the HCS + MM products were hydrides, they were dehydrogenated completely by evacuating upon being heated to 603 K at a heating rate of 5 K/min prior to the hydriding kinetics measurement. Then, the hydriding kinetics at different temperatures was measured under the initial hydrogen pressure of 3.0 MPa. The dehydriding kinetics was measured under vacuum at 473 K, and 0.005 MPa hydrogen pressure at temperatures higher than 523 K.

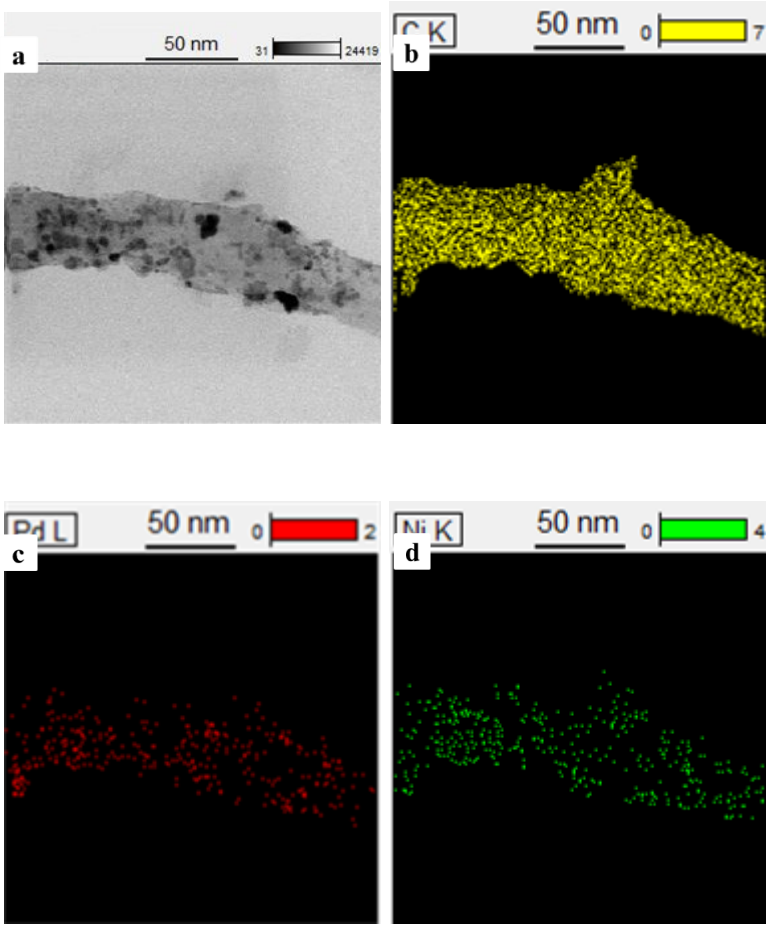

Fig. S1 TEM images of Pd_3Ni_3/MWCNTs$_4$ catalyst: (a) bright field image; (b-d) EDS mapping of C, Pd and Ni coincided with (a)

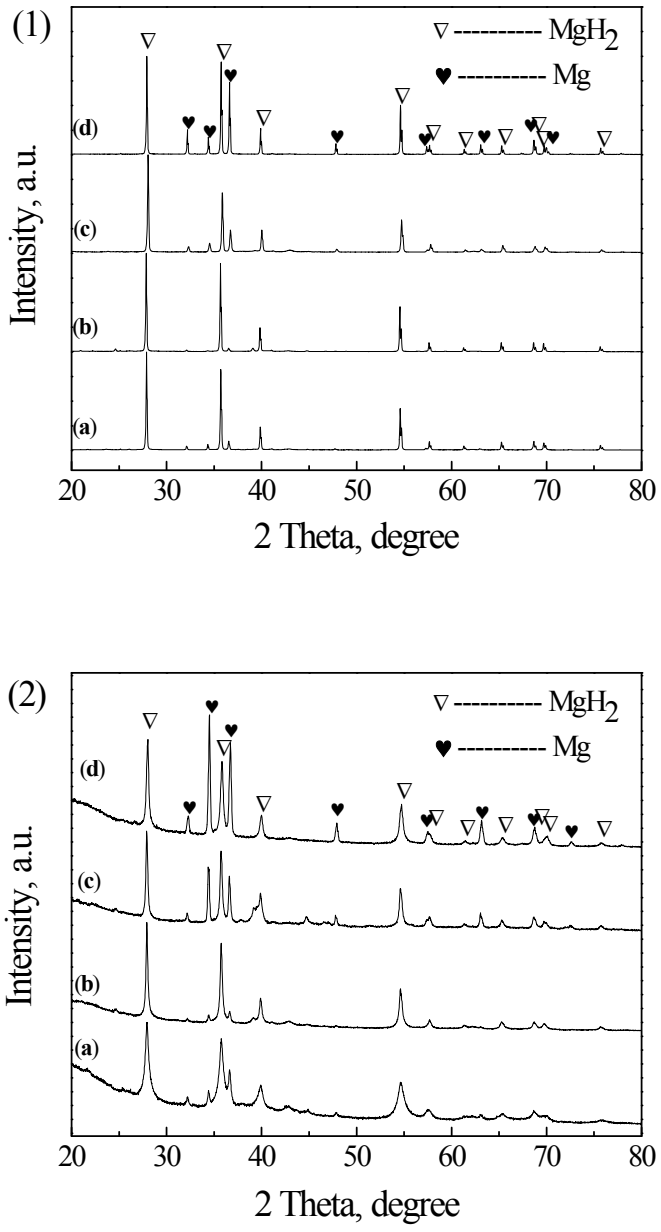

Fig. S2 XRD patterns of the HCS products (1) and HCS+MM products (2): (a) Mg_{95}-$(Pd_3Ni_3/MWCNTs_4)_5$, (b) Mg_{95}-$(Pd_6/MWCNTs_4)_5$, (c) Mg_{95}-$(Ni_6/MWCNTs_4)_5$, and (d) Mg

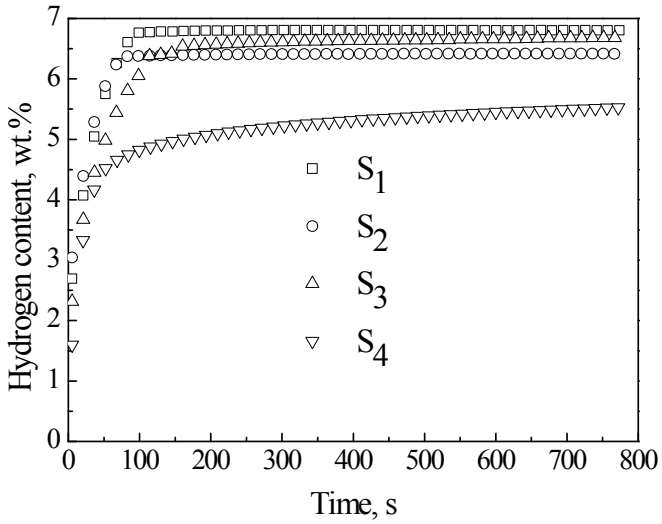

Fig. S3 Hydriding curves of the HCS+MM products: S1 Mg_{95}-(Pd_3Ni_3/$MWCNTs_4$)$_5$, S2 Mg_{95}-(Ni_6/$MWCNTs_4$)$_5$, S3 Mg_{95}-(Pd_6/$MWCNTs_4$)$_5$ and S4 Mg under the initial hydrogen pressure of 3.0 MPa at temperature of 523 K

Table S1 Comparison of the hydrogen absorption capacities within 800 s of the HCS+MM products of Mg_{95}-(Pd_3Ni_3/$MWCNTs_4$)$_5$, Mg_{95}-(Ni_6/$MWCNTs_4$)$_5$, Mg_{95}-(Pd_6/$MWCNTs_4$)$_5$ and Mg measured at different temperatures of 373 K, 473 K and 523 K under 3.0 MPa hydrogen pressure

Temperature (K)	Hydrogen absorption capacity (wt.%)			
	Mg_{95}-(Pd_3Ni_3/ $MWCNTs_4$)$_5$	Mg_{95}-(Ni_6/ $MWCNTs_4$)$_5$	Mg_{95}-(Pd_6/ $MWCNTs_4$)$_5$	Mg
373	6.44	5.93	0.18	0
473	6.79	6.44	6.66	3.45
523	6.80	6.42	6.68	5.53

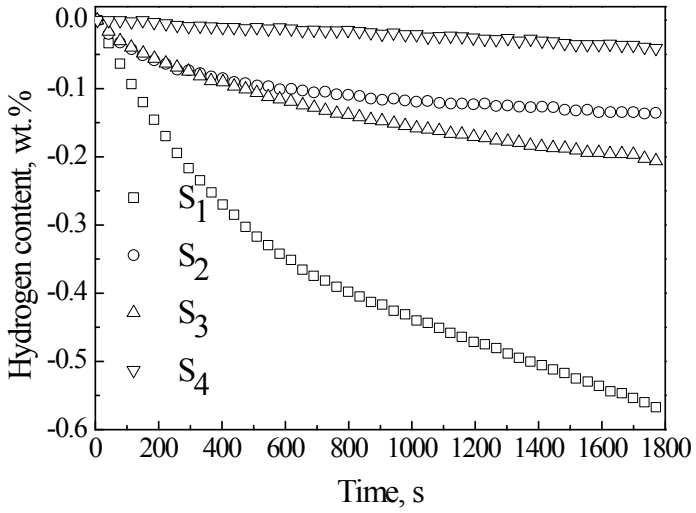

Fig. S4 Dehydriding curves of the HCS+MM products: S1 Mg_{95}-(Pd_3Ni_3/$MWCNTs_4$)$_5$, S2 Mg_{95}-(Ni_6/$MWCNTs_4$)$_5$, S3 Mg_{95}-(Pd_6/$MWCNTs_4$)$_5$ and S4 Mg under vacuum at temperature of 473 K.

Table S2 Comparison of the hydrogen desorption capacities within 1800 s of the HCS+MM products of Mg_{95}-(Pd_3Ni_3/$MWCNTs_4$)$_5$, Mg_{95}-(Ni_3/$MWCNTs_2$)$_5$, Mg_{95}-(Pd_3/$MWCNTs_2$)$_5$ and Mg measured at 473 K under vacuum, at 523 K and 573 K under 0.005 MPa hydrogen pressure

Temperature (K)	Hydrogen desorption capacity (wt.%)			
	Mg_{95}-(Pd_3Ni_3/ $MWCNTs_4$)$_5$	Mg_{95}-(Ni_6/ $MWCNTs_4$)$_5$	Mg_{95}-(Pd_6/ $MWCNTs_4$)$_5$	Mg
473	0.57	0.14	0.21	0.04
523	6.41	3.80	0.52	0.14
573	6.70	5.88	6.27	4.09

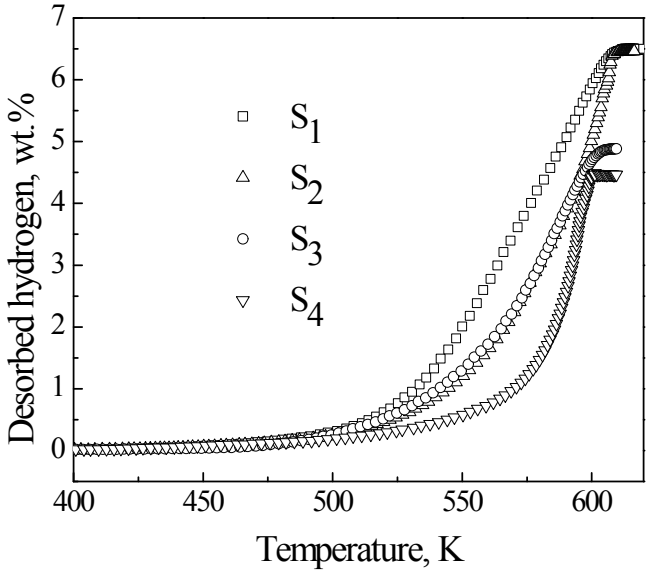

Fig. S5 The amount of hydrogen desorbed as a function of temperature of the HCS+MM products: S1 Mg_{95}-(Pd_3Ni_3/$MWCNTs_4$)$_5$, S2 Mg_{95}-(Ni_6/$MWCNTs_4$)$_5$, S3 Mg_{95}-(Pd_6/$MWCNTs_4$)$_5$ and S4 Mg. (the average heating rate was 20 K/min)

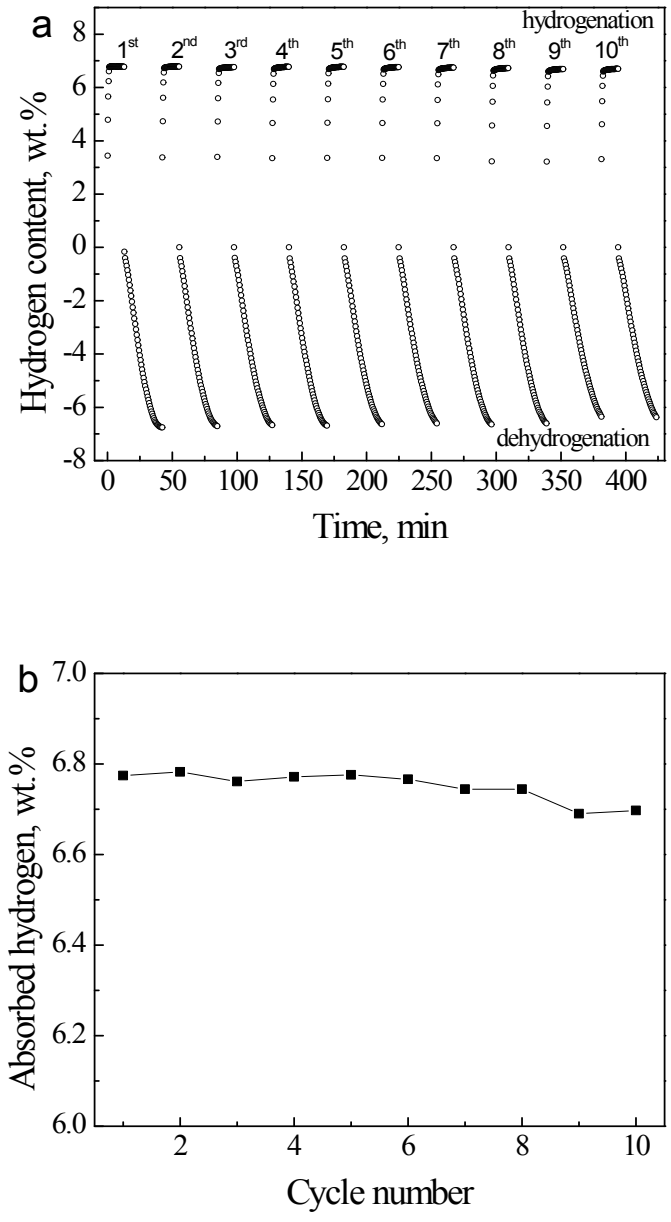

Fig. S6 (a) Isothermal hydrogenation and dehydrogenation cyclic kinetics curves of the HCS+MM-Mg_{95}-(Pd_3Ni_3/MWCNTs$_4$)$_5$ composite from the 1st cycle to the 10th cycle at 528 K; (b) The cyclic hydrogen absorption capacity of the composite as a function of cycle number.

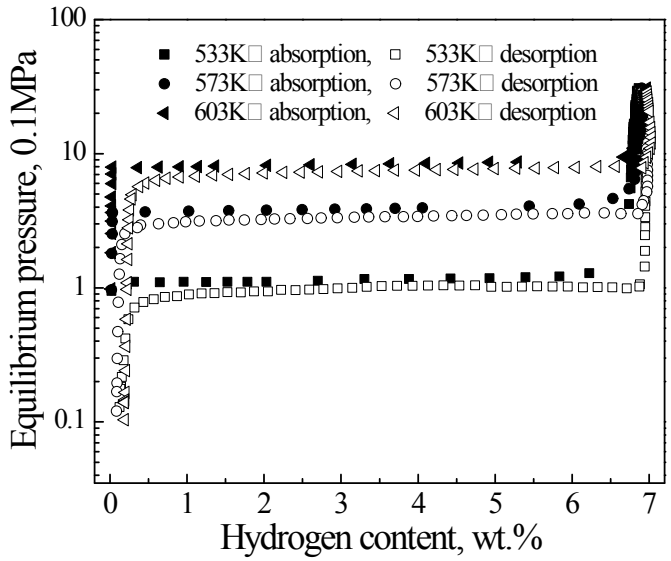

Fig. S7 Hydrogen absorption/desorption PCT curves of the HCS+MM-Mg_{95}-$(Pd_3Ni_3/MWCNTs_4)_5$ composite measured at different temperatures of 533, 573 and 603 K, respectively

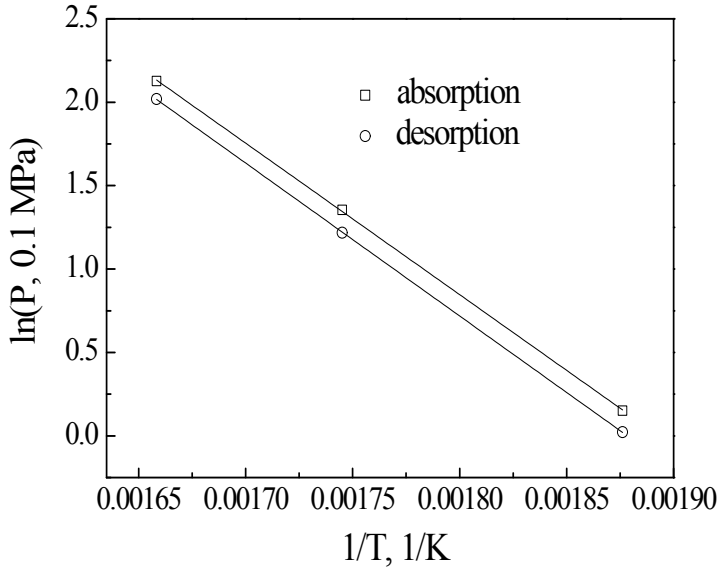

Fig. S8 Van't Hoff plot for hydrogen absorption/desorption of Mg in the HCS+MM- Mg_{95}-$(Pd_3Ni_3/MWCNTs_4)_5$ composite

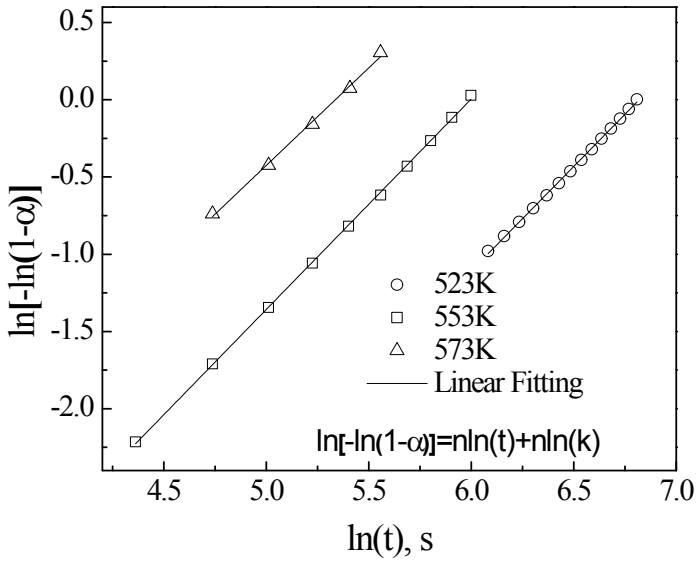

Fig. S9 JMA plots of ln[−ln(1−α)] *vs* ln(t) for the dehydrogenation of the HCS+MM- Mg_{95}-$(Pd_3Ni_3/MWCNTs_4)_5$ composite at different temperatures. The samples with reacted fraction of $0.1 < \alpha < 0.7$ was used

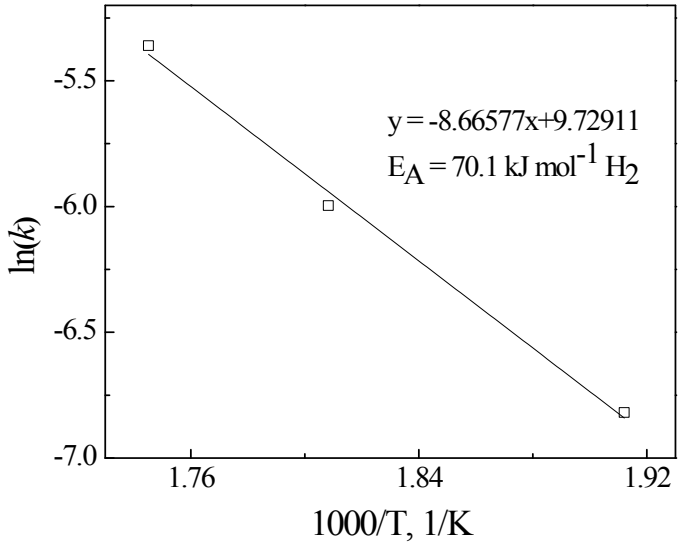

Fig. S10 Arrhenius plots for the dehydriding kinetics of the HCS+MM-Mg_{95}-$(Pd_3Ni_3/MWCNTs_4)_5$ composite

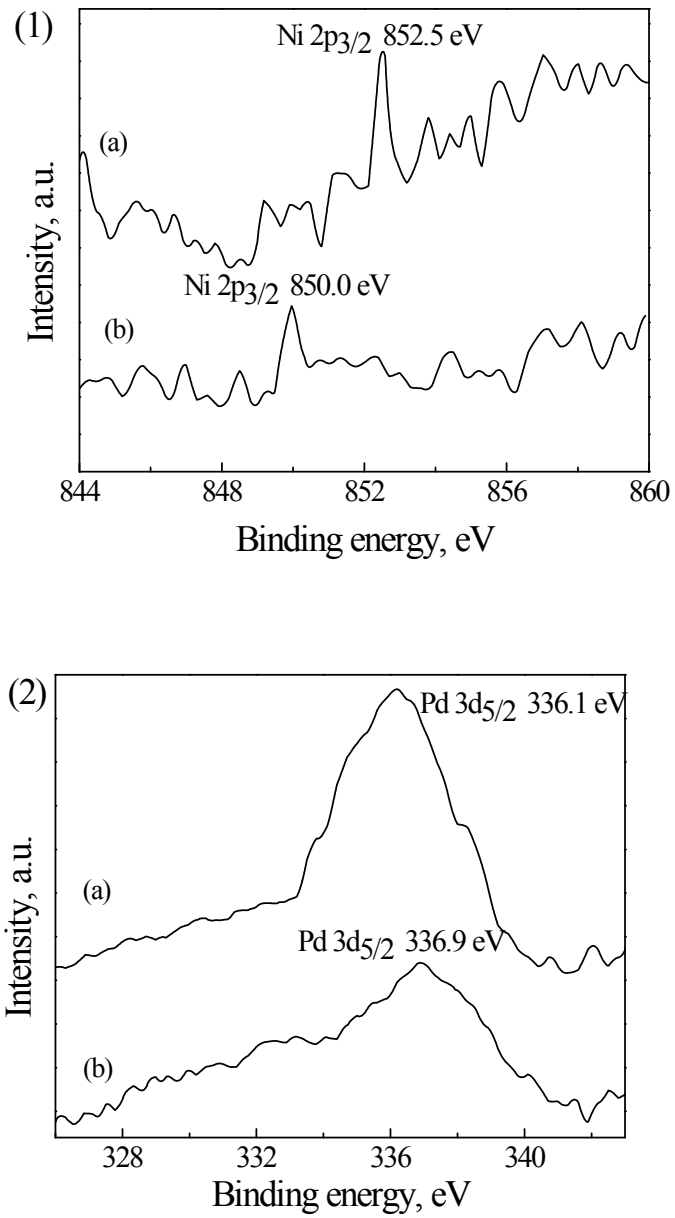

Fig. S11 XPS spectra of Ni $2p_{3/2}$ and Pd $3d_{5/2}$ for the HCS+MM-Mg_{95}-$(Pd_3Ni_3/MWCNTs_4)_5$ composite in the dehydrogenated (a) and hydrogenated (b) states

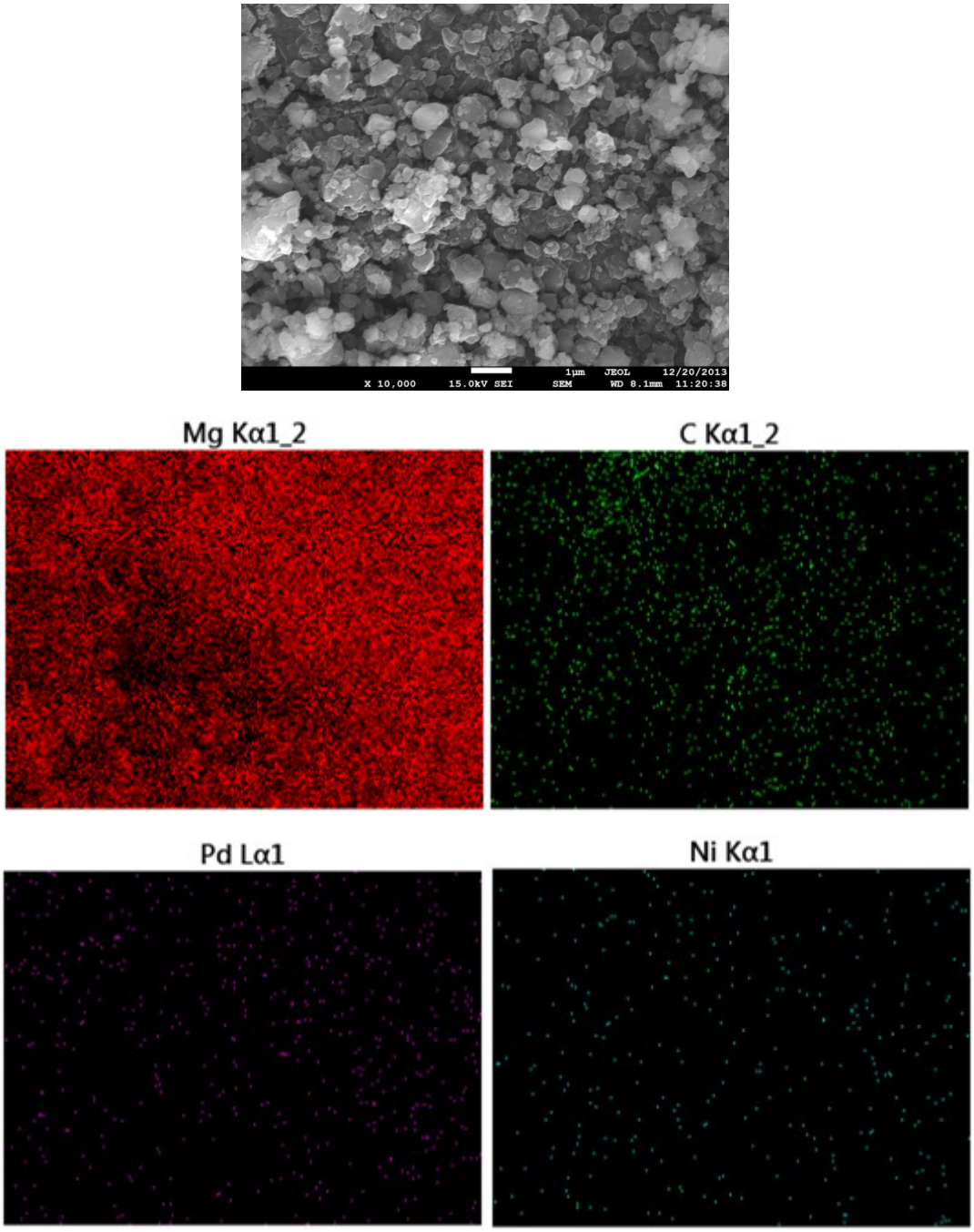

Fig. S12 SEM image of the HCS+MM-Mg_{95}-$(Pd_3Ni_3/MWCNT_4)_5$ composite with associated EDS maps for (a) Mg (b) C (c) Pd and (d) Ni